metals

MDPI

Article

Peculiar Spatiotemporal Behavior of Unstable Plastic Flow in an AlMgMnScZr Alloy with Coarse and Ultrafine Grains

Daria Zhemchuzhnikova [1,*], Mikhail Lebyodkin [1], Tatiana Lebedkina [2,3], Anna Mogucheva [4], Diana Yuzbekova [4] and Rustam Kaibyshev [4]

1 Laboratoire d'Etude des Microstructures et de Mécanique des Matériaux (LEM3), CNRS UMR 7239, Université de Lorraine, 7 rue Félix Savart, BP 15082, 57073 Metz CEDEX 03, France; mikhail.lebedkin@univ-lorraine.fr

2 Center of Excellence "LabEx DAMAS", Université de Lorraine, 7 rue Félix Savart, 57073 METZ, France; tatiana.lebedkin@univ-lorraine.fr

3 Togliatti State University, Belorusskaya St. 14, Tolyatti 445020, Russia

4 Laboratory of the Mechanical Properties of Nanoscale Materials and Superalloys, Belgorod State University, Pobedy Street 85, Belgorod 308015, Russia; mogucheva@bsu.edu.ru (A.M.); yuzbekova@bsu.edu.ru (D.Y.); rustam_kaibyshev@bsu.edu.ru (R.K.)

* Correspondence: daria.zhemchuzhnikova@univ-lorraine.fr; Tel.: +33-(0)3-72-74-78-49

Received: 20 July 2017; Accepted: 18 August 2017; Published: 23 August 2017

Abstract: The work addresses the effects of nanosize particles and grain refinement on the patterns of stress serrations and kinematics of deformation bands associated with the Portevin–Le Chatelier instability of plastic flow. Ultra-fine-grained microstructure was obtained using equal-channel angular pressing of the initial coarse-grained alloy. Tensile tests were carried out on flat specimens at strain rates in the range from 3×10^{-5} to 1.4×10^{-2} s^{-1}. Using local extensometry techniques, it was found that the presence of nanoscale precipitates promotes quasi-continuous propagation of deformation bands in the entire strain-rate range. The grain refinement leads to a transition to relay-race propagation at high strain rates and static strain localization at low rates. The results are discussed from the viewpoint of competition between various dynamical modes of plastic deformation associated with collective dynamics of dislocations.

Keywords: aluminum alloys; precipitates; severe plastic deformation; mechanical characterization; Portevin–Le Chatelier effect; deformation bands; collective dislocation dynamics

1. Introduction

The elaboration of new alloys sustains strong interest to the phenomenon of unstable plastic flow, or the Portevin–Le Chatelier (PLC) effect [1], caused by interaction of dislocations with solute atoms. The plastic instability manifests itself as strain localization in deformation bands giving rise to serrations on the stress-strain curves [2]. Such localization can have detrimental consequences on the production and utilization of industrial pieces, in particular, because of the formation of traces on the surface of the product and a reduced ductility. The microscopic mechanism of the PLC effect is understood rather well in terms of the dynamic strain aging (DSA) responsible for alternating pinning and release of mobile dislocations by atmospheres of solute atoms [3–7]. However, its macroscopic behavior is associated with complex patterns of stress serrations related to nucleation and motion of deformation bands in the deforming material and requires understanding of self-organization of dislocations [8,9].

Plastic deformation of Al-based alloys is prone to instability in a wide range of experimental conditions [10]. Binary Al-based alloys, especially 5000 series with Mg as the main impurity,

were used for a long time as model materials for investigation of the PLC effect (e.g., [7–16]). Spatiotemporal behavior of tensile deformation of such alloys fits well the phenomenological classification based on three frequently observed types [2]. In binary Al-Mg alloys, all these types are observed depending on temperature and strain rate. At a given temperature, type *A* occurs close to the high strain-rate boundary of the domain of instability. It is characterized by deformation bands propagating along the tensile axis. The deformation curves display rises in stress required to nucleate a band. The formation of a band produces a stress drop followed by smoother flow during the band propagation. When the strain rate is reduced, type *A* is replaced by type *B* behavior characterized by relatively regular abrupt stress oscillations. They are caused by a brief occurrence of immobile bands in an ordered manner, so that this behavior is referred to as a relay-race or hopping propagation. This pattern provides an additional signature of type *B* serrations because the passage of a series of bands through the sample corresponds to a packet of regular stress serrations at a similar stress level, followed by an increase in the stress required to start a new relay-race in the work-hardened material. The further decrease in the strain rate leads to less regular and usually very deep and abrupt stress drops of type *C* associated with almost unordered deformation bands [17].

This phenomenology has been successfully explained from the viewpoint of collective behavior of dislocations [8,9,18]. However, the above-described patterns cannot be simply extended to alloys with a more complex composition. The main disadvantage of binary Al-Mg alloys is their low yield stress. A significant strength increase can be achieved by additional alloying, in particular, leading to precipitation [19,20]. It occurs that the additional strong obstacles to the motion of dislocations may affect their collective dynamics. Although mechanical characteristics of Al-Mg alloys containing a dispersion of secondary phases were intensely studied, the peculiarities of spatiotemporal behavior of their plastic deformation have attracted attention only recently. It was shown [21] that the domain of instability of an Al-Mg alloy containing coherent Al_3(Sc,Zr) dispersoids is shifted to the range of high strain rates. Importantly, the band propagation regime was found to persist over the entire strain-rate range, even at the lowest strain rate corresponding to stress serrations of type *C*. Such behavior was not reported for binary alloys, nor predicted by the existing models of the PLC effect.

The other way to produce high-strength materials is an extensive grain refinement by severe plastic deformation [22–24]. However, there exists very limited information on the PLC instability in fine-grained materials, which in addition is contradictory [24–27]. For example, grain refinement was reported to suppress the PLC effect in dilute Al-Mg alloys [26,27]. In contrast, an extension of the instability domain towards lower strain rates resulting in higher-amplitude serrations was observed in alloys containing non-shearable nanoscale precipitates [24,25]. Furthermore, the grain boundaries and precipitates may provide a synergetic effect on the spatial coupling between local strains and the conditions of self-organization of dislocations. However, until now there have been no reports on the relationship between the occurrence of different serration patterns and the spatial activity of PLC bands in such materials. The objective of the present paper was to examine specific features of spatiotemporal behavior of PLC bands in an AlMgMnScZr alloy with nanoscale coherent precipitates, for different grain sizes and strain rates.

2. Materials and Methods

The details of the alloy manufacturing procedure, the initial microstructures, and the overall mechanical properties of the investigated material were described elsewhere [25,28] and will be briefly outlined here. The 5024 alloy with a chemical composition of Al-4.57Mg-0.35Mn-0.2Sc-0.09Zr (wt. pct.) was produced by continuous casting. The ingot was then subjected to solution treatment followed by hot extrusion. The resulting microstructure will be denoted hereinafter as coarse-grained (CG) condition. To obtain ultra-fine-grained (UFG) material, rectangular samples with dimensions of $20 \times 20 \times 100$ mm^3 were machined from the central part of the extruded ingot parallel to the extrusion direction and subjected to equal-channel angular pressing (ECAP) to a total strain ~12 at a temperature of 300 °C using route B_C [28,29].

Tensile samples with the gage section of $35 \times 7 \times 3$ mm^3 were cut parallel to either the extrusion or pressing direction. Tension tests were performed at room temperature and constant grip velocity corresponding to the nominal applied strain rate r_a ranging from 3×10^{-5} to 1.4×10^{-2} s^{-1}.

Two different techniques were used to examine behavior of the PLC bands. First, a local extensometry technique was applied to visualize the evolution of a one-dimensional (along the tensile axis) local strain field. This method is based on the recording of displacements of markers that are deposited on the specimen surface by painting a grid of black and white stripes normal to the tensile axis (see [21,30] for details). The pairs of markers form about twenty 1 mm wide local extensometers. The high spatial (1.3 μm) and time (1 ms) resolution of the CCD (charge-coupled device) camera used for these measurements provided a high-accuracy determination of local strain rates. Although 1D method does not allow for observing the deformation bands shape, it has an advantage of visualization of the time evolution of their positions along the specimen axis. This objective is attained by constructing 3D maps which display local strain rates as functions of time and coordinates of the extensometers. Such maps facilitate the detection of transitions between different band patterns, as well as estimation of the band width and velocity. A current drawback of this technique is that the recording equipment limits the record duration by ten minutes, making it impractical for r_a below 10^{-4} s^{-1}.

The second technique, based on 2D digital image correlation (DIC), did not have such limitation of the test duration and was applied at $r_a = 3 \times 10^{-5}$ s^{-1}. For this, one specimen surface was painted white and then a speckle pattern was deposited onto it using a spray of black paint. A 2D digital camera recorded consecutive images of the entire gage part of the specimen with a rate of 1 frame per 65 ms and spatial resolution about 25 pixels per mm. The local strain-rate field was calculated with the aid of the standard image correlation software, Vic-2D. Although the time resolution of this method is worse than in the above-described case, it has advantages of visualization of the shape of the deformation band and a smaller discreteness corresponding to a mesh-size about 0.1 mm [31].

3. Results

3.1. Microstructure before and after ECAP

The CG state of the alloy was characterized by coarse grains with the mean size of approximately 20 and 200 μm along the transverse and longitudinal directions, respectively, and the lattice dislocation density close to 10^{13} m^{-2} (cf. [28]). The main secondary phase was represented by coherent dispersoids of an Al_3(Sc,Zr)-phase with average size about 10–15 nm and equiaxed shape. Figure 1a presents a TEM microphotograph of a part of a grain which reveals that such precipitates are uniformly distributed within the grain interiors. Several dislocation segments can also be seen.

ECAP resulted in the formation of a fully recrystallized structure composed of equiaxed grains with the size reduced to less than 1 μm. The fraction of high-angle boundaries (HAB) and the mean misorientation amounted to 70% and 30°, respectively. An example of a TEM microphotograph of an area containing several grains is presented in Figure 1b. The dislocation density was increased by more than an order of magnitude. No visible effect of ECAP on the size or distribution of Al_3(Sc,Zr) dispersoids was found (see also [28]).

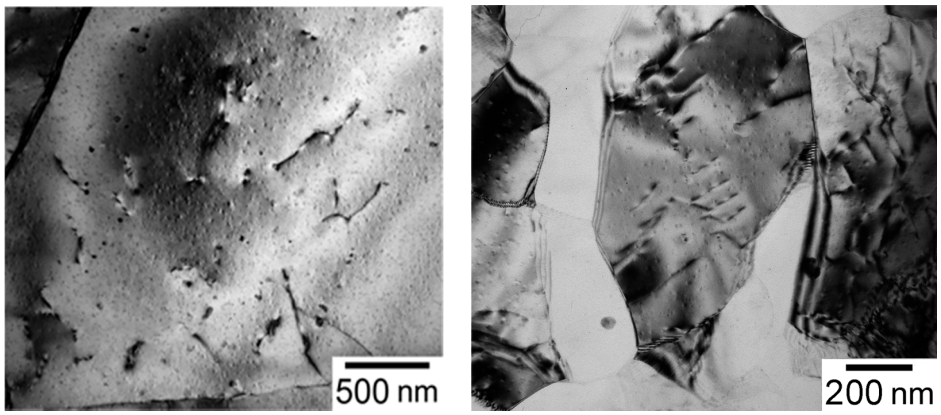

Figure 1. Initial microstructure of the 5024 alloy: (**a**) coarse-grained state; (**b**) after 12 equal-channel angular pressing (ECAP) passes.

3.2. Stress Serrations Patterns

Examples of deformation curves of the 5024 alloy in two grain structure conditions are presented in Figure 2 for strain rates in the range of 1.4×10^{-4} to 1.4×10^{-2} s^{-1}. As far as macroscopic mechanical behavior is concerned, it can be seen that the grain refinement does not affect the ductility of the investigated material although the features of the unstable flow change strongly. All deformation curves exhibit stress serrations. The comparison of the average stress levels at different strain rates shows that the flow stress generally decreases when the strain rate is increased (see also [25]). This trend agrees with the requirement of negative strain-rate sensitivity (SRS) in the DSA theory, as a necessary condition of plastic instability. However, the strength variation between samples was considerable, especially after ECAP [24–28]. Consequently, quantitative estimations of the SRS were not performed in the present work.

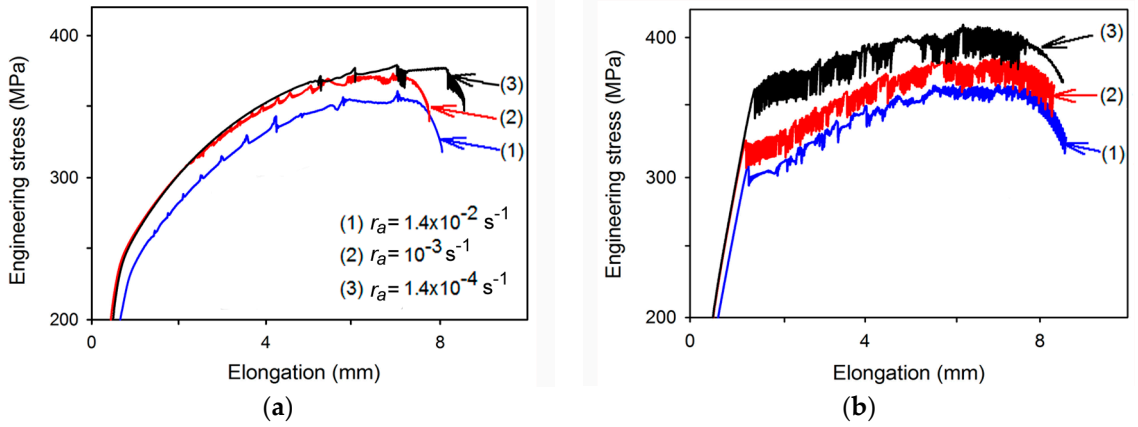

Figure 2. Typical deformation curves of the 5024 alloy: (**a**) coarse-grained state; (**b**) after 12 ECAP passes. The values of the imposed strain-rate indicated in plot (**a**) are common for both plots.

At first sight, the CG alloy globally displays well-known features of serrated deformation curves (cf. Section 1). Nevertheless, some peculiarities described below, in particular, with regard to the usual sequence of types of serrations, testify changes in the dynamical behavior of the PLC effect, as corroborated by the analysis of the deformation band kinematics in Section 3.3. The plastic flow becomes unstable beyond some critical strain which follows the so-called inverse dependence on the strain rate, i.e., it decreases when the strain rate is increased [21,32,33]. Like in binary Al-Mg alloys, the serrations show a clear type *A* shape at the high strain rate, $r_a = 1.4 \times 10^{-2}$ s^{-1} (Figure 2a,

curve (*1*)). When r_a is decreased to 10^{-3} s^{-1}, type *A* serrations also occur over a large portion of the deformation curve, while a mixture of types *A* and *B* can be seen at large strains (Figure 2a, curve (2)). However, the transition to pure type *B* behavior does not take place even when the strain rate is further decreased. As can be recognized on curve (*3*), the serrations acquire type *C* shape at 1.4×10^{-4} s^{-1}, with a peculiarity of displaying very long smooth intervals between deep stress drops. Finally, stable plastic flow was found at $r_a = 3 \times 10^{-5}$ s^{-1}. On the whole, these patterns resemble results [21] for an alloy with a similar chemical composition.

In the UFG material with a fully recrystallized microstructure, discontinuous yielding [34,35] takes place. Serrations start immediately upon the elastoplastic transition (Figure 2b). Such a reduction in the critical strain in a material with a high initial dislocation density is consistent with the DSA mechanism [36]. More puzzling is how drastically the ECAP treatment modifies the serration patterns. In contrast to the CG material, deep stress drops of type *B* are dominant at high and intermediate $\dot{\varepsilon}_a$-values, even if features of type *A* are observable at the highest r_a. Intervals of smoother flow between deep stress drops, indicating a transition to type *C* behavior, appear when r_a is decreased to 1.4×10^{-4} s^{-1}. This transition is completed at the strain rate of 3×10^{-5} s^{-1} characterized by clear type *C* serrations (Figure 3). The entirety of the data corroborates the earlier observation that the lower boundary of instability may be extended towards lower r_a upon grain refinement [25].

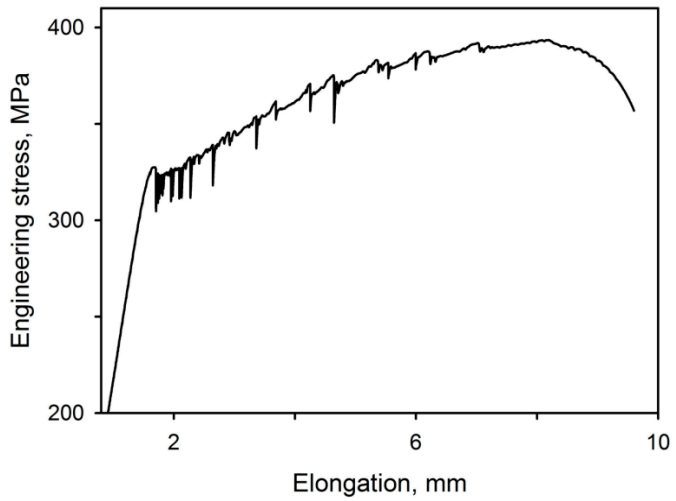

Figure 3. Example of a deformation curve for the ultra-fine-grained (UFG) alloy tested at $r_a = 3 \times 10^{-5}$ s^{-1}.

Another distinct feature of the material processed by ECAP is the Lüders-like plateau [25,34,35] following the elastoplastic transition and superimposed with stress drops (Figure 2b). The formation of the Lüders plateau is well documented for Al-Mg alloys (e.g., [37,38]) and is generally explained by the nucleation and propagation of a deformation band. In contrast to the repetitive PLC bands, the Lüders band propagates once, as a result of unpinning of dislocations from solute atmospheres formed during static aging prior to deformation [34,35]. This process occurs virtually without increasing the stress level because the band advances into the unhardened material. The presence of stress serrations during the Lüders plateau in Figure 2b suggests that it does not correspond to a continuous propagation but to a relay race, in agreement with the persistence of type *B* behavior during the whole test.

3.3. PLC Bands Patterns

The main features of deformation bands behavior for different grain structures and strain rates are synthesized in Figures 4–8. Figures 4–7 represent spatiotemporal patterns obtained with the aid of the 1D local extensometry that allows for continuous recording of the positions of markers along

the specimen axis. Figure 8 was obtained using DIC technique. It displays several instantaneous 2D images of deformation bands.

Like the deformation curves, the spatiotemporal patterns found in the CG state are also globally similar to those reported in [21] for a similar alloy. Their main feature is the persistent propagation of deformation bands at all strain rates, as contrasted with the well-known transitions between three types of behavior characterizing binary Al-Mg alloys. Moreover, while in [21] a tendency to the transition from the continuous to relay-race propagation regime was detected at intermediate strain rates, almost no footprint of relay-race propagation was found in the present work. Figure 4 illustrates the continuous propagation of deformation bands at $r_a = 10^{-3}$ s^{-1}, in conformity with type *A* [14,39] character of the deformation curve. To better understand this map, it should be clarified that during the tensile test, some bottom markers leave the field of vision of the CCD camera and some top markers enter it, so that only a part of them are constantly surveyed during a given time interval. So, only a 14 mm long part of the gage length is represented in Figure 4. It can be seen that each deformation band is nucleated outside the surveyed part and continues propagating after having passed it. Consequently, the visible intervals of propagation are shorter than the smooth periods between the stress rises corresponding to the bands nucleation. The instants of band nucleation can be guessed, though, due to dark spots which indicate local compressions caused by the elastic reaction ("spring-back") of the material outside the deformation band. The band velocity V ranges from several mm/s at 10^{-3} s^{-1} to several tens mm/s at 1.4×10^{-2} s^{-1} and slows down during the test (V is simply the slope of the traces in Figure 4). The maximum local strain rate within the deformation band, r_{loc}, exceeds r_a by a factor κ varying approximately between 7 and 10, a value typical of type *A* behavior in Al-Mg alloys [40].

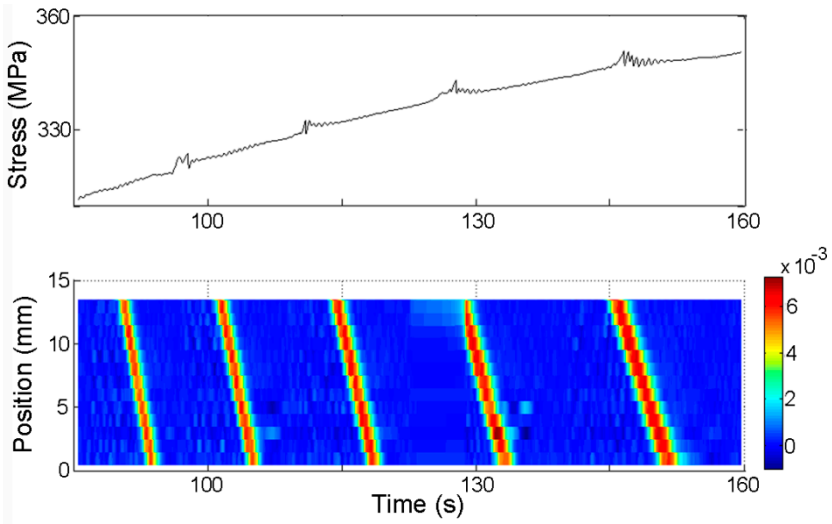

Figure 4. Spatiotemporal pattern showing the time evolution of the local strain rate along the tensile axis of a sample of the coarse-grained (CG) alloy. $r_a = 10^{-3}$ s^{-1}. Color bar quantifies the local strain-rate scale in s^{-1}.

Figure 5 characterizes spatiotemporal behavior observed at the low strain rate. Details of the initial part of plastic flow illustrated in plots (b) and (c) show that whereas the deep stress drops expectedly correspond to brief occurrence of static deformation bands characteristic of type *C*, the following smooth intervals are not related to a macroscopically uniform flow but to the continuous propagation of a deformation band. The properties of such bands correspond to the properties of deformation bands observed at higher strain rates: their velocity is decreased in proportion to the r_a value; κ is approximately 7. Besides, the κ-ratio indicates that the static deformation bands are quantitatively different from the usual type *C* bands. Indeed, while κ is expectedly higher in the

static bands than in their moving counterparts, it only reaches the value about 20. It is at least two orders of magnitude lower than that reported in [40] for type *C* bands in a dilute Al-4.5wt %Mg alloy. The visualization of spatiotemporal patterns thus testifies to strongly modified behavior of deformation bands at the low strain rate, which manifests a mixture of type *C* and type *A* features.

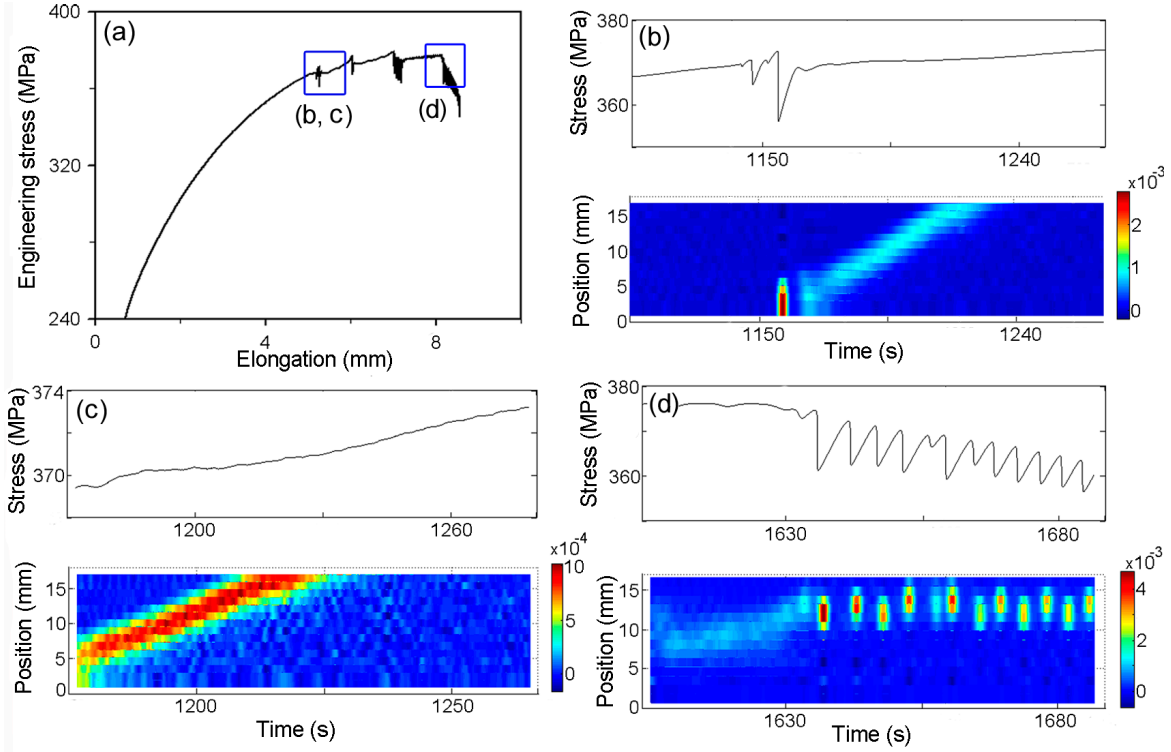

Figure 5. (**a**) Deformation curve recorded at 1.4×10^{-4} s^{-1} in the CG state and the corresponding strain-rate maps for the strain intervals denoted by rectangles: (**b**) Time interval covering the nucleation of a band and its following propagation; (**c**) Portion of plot (**b**) corresponding to the band propagation; (**d**) Oscillating deformation curve observed during necking and the repetitive strain localization responsible for these serrations.

Finally, Figure 5d indicates that necking behavior is impacted by the PLC effect (cf. [41]). The onset of necking occurs through slowing down and immobilization of a PLC band. The following development of the neck does not correspond to a steadily intensifying shear band but proceeds through plastic instability similar to type *C* behavior, although certain differences with the above-described kinematics of the PLC bands of type *C* are noteworthy. The κ-ratio tends to decrease from ~50 at the onset of necking to ~20 while the necking proceeds. The deformation bands are constrained to the necked region, even if they slightly shift forth and back along the specimen axis. The final rupture is related to the repeated localization of plastic deformation in the same cross-section of the specimen. A detailed study of necking goes beyond the scope of this paper and will be reported elsewhere.

Grain refinement led to qualitative changes in these patterns. Figure 6 represents high strain-rate behavior of the UFG material. As could be anticipated from the deformation curves, type *B* behavior is preponderant in this case, even if it is difficult to distinguish between quasi-continuous and relay-race propagation at the highest $r_a = 1.4 \times 10^{-2}$ s^{-1} (Figure 6a). The distinct relay race is fully established at 10^{-3} s^{-1} in Figure 6b. Moreover, in contrast to the continuous propagation cases in Figures 4 and 5, κ-value exceeds 15 and 50, respectively, at 1.4×10^{-2} and 10^{-3} s^{-1}.

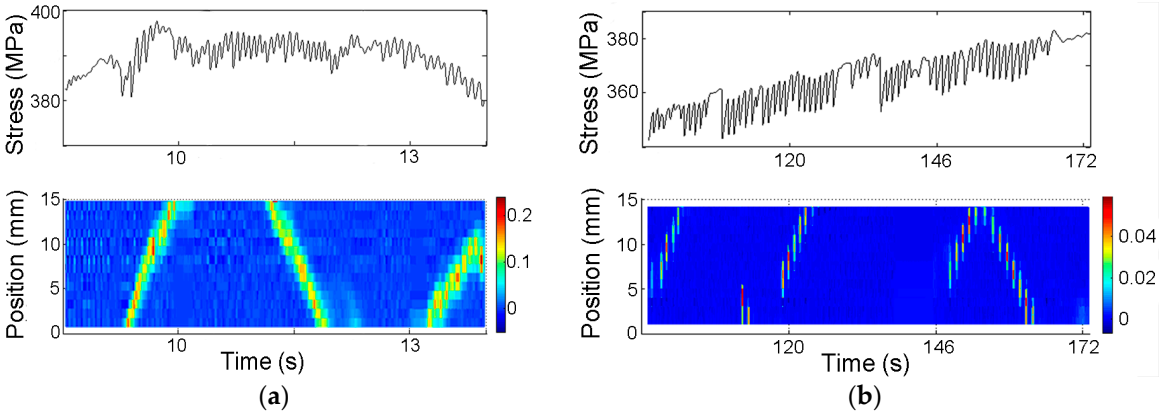

Figure 6. Similar maps for samples of the alloy subjected to 12 ECAP passes: (**a**) $r_a = 1.4 \times 10^{-2}$ s^{-1}; (**b**) $r_a = 10^{-3}$ s^{-1}.

The spatial aspect illustrated in Figure 7 for $r_a = 1.4 \times 10^{-4}$ s^{-1} confirms the suggestion of the starting transition from type *B* to type *C* behavior made in Section 3.2. Indeed, Figure 7b displays pairs of deformation bands occurring alternatively between the regions inside and outside the field of vision (Figure 7b manifests rather strong spring-back effect in the region of the elastoplastic transition. It is likely to be due to the fact that the plastic flow has not yet started all over the specimen); the tendency to a relay race (Figure 7c) alternates with uncorrelated nucleation of deformation bands; κ becomes as high as 150; the strain interval close to the onset of necking displays bands hopping forth and back until practically steady strain localization (Figure 7d). On the whole, in contrast to Figure 4 that displays spatiotemporal patterns for CG material at the same strain rate, no continuous band propagation was detected for the UFG material.

This conclusion is corroborated by the results of DIC imaging at the strain rate of 3×10^{-5} s^{-1} corresponding to well-established type *C* serrations represented in Figure 3. Figure 8 displays the initial portion of this deformation curve and four DIC images corresponding to the instants of stress serrations. The vertical rectangles are images of the distribution of the local strain rate almost over the entire gage part of the sample approximately 30×7 mm^2 in size. The numbers above the rectangles indicate the maximum r_{loc} within each image. It can be seen that the stress drops at the instants t_1 to t_4 are caused by deformation bands which form an angle about 60° with the tensile axis, characteristic of PLC bands (see, e.g., [12,16]). These bands do not follow a relay race sequence and are characterized by a very high κ between 750 and 900, i.e., more than an order of magnitude higher than the values found for type *B* bands (cf. Figure 6). The rest of the image appears as a uniform background because the powerful PLC bands dominate the contrast. It should be strengthened that contrarily to CG material, no propagation of PLC bands was found during smooth portions of the deformation curve between stress serrations. These periods thus correspond to an approximately uniform plastic flow. The entire spatiotemporal pattern corresponds to usual type *C* behavior.

Finally, the above-used notion of a macroscopically uniform plastic flow deserves some clarification. It is known that low-amplitude heterogeneities having a wavy or intermittent character accompany "smooth" deformation of various materials including polycrystalline alloys and pure single crystals [42–44]. In the present work, too, rich patterns of such heterogeneities were found at a fine scale of local strain rates in both CG and UFG conditions of the 5024 alloy. However, they represent much weaker effects in comparison with the PLC instability and will be reported elsewhere.

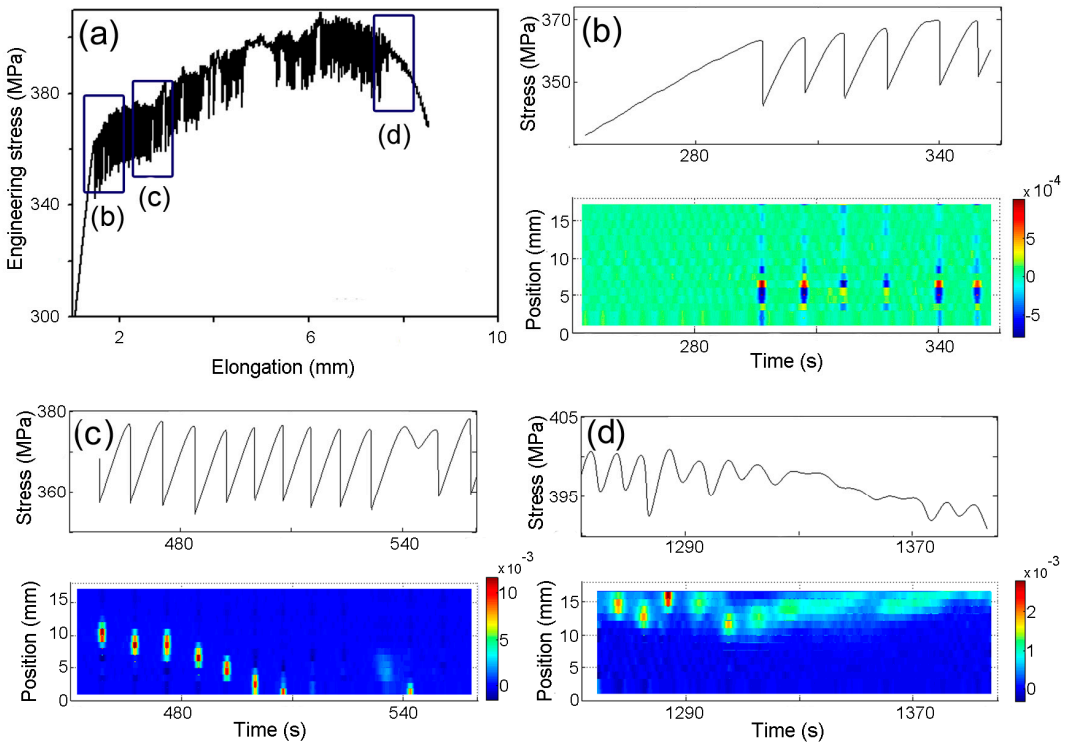

Figure 7. (**a**) Deformation curve recorded at 1.4×10^{-4} s^{-1} for the alloy after 12 ECAP passes; (**b**–**d**) the corresponding strain-rate maps for the strain intervals denoted by rectangles in plot (**a**).

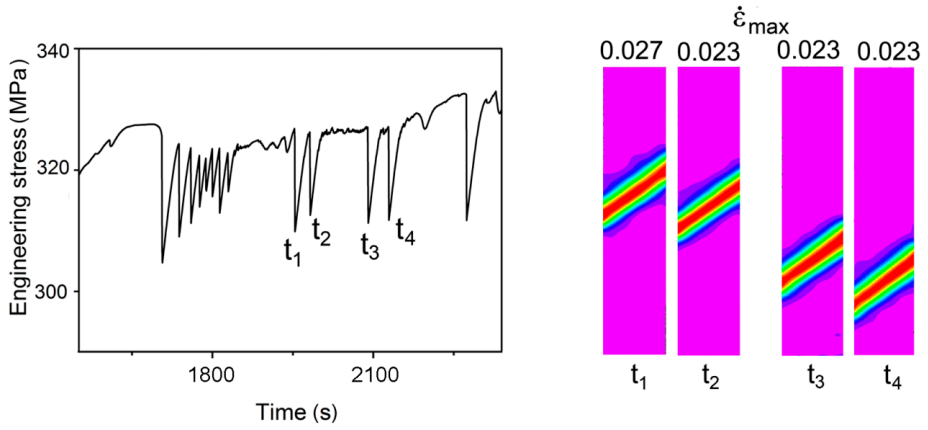

Figure 8. Initial portion of the deformation curve shown in Figure 2 and digital image correlation (DIC) images of the distribution of the local strain rate over the gauge part of the sample. The DIC images are recorded at the instants indicated on the deformation curve. The maximum value of the local strain rate within the band is indicated at the top of each snapshot.

4. Discussion

Inspection of the experimental data shows that the initial microstructure significantly affects both the deformation curves and kinematics of deformation bands in the 5024 alloy. An unusual feature of the PLC effect observed in the CG condition is that the quasi-continuous mode of deformation band propagation (type *A* behavior) persists over the entire strain-rate domain of plastic instability, whereas the well-known behavior suggests a transition to relay-race propagation (type *B*) and then to static deformation bands (type *C*) when the imposed strain rate is decreased. Such persistence of the propagation was recently observed in an alloy with a similar phase composition containing

a dispersion of nanoscale coherent Al_3(Sc,Zr) precipitates [21]. The fact that both alloys display the same peculiarities suggests the existence of an inherent mechanism related to the presence of nanoscale precipitates. A possible explanation was proposed in [21] in terms of stress concentration on the precipitates. It was suggested that as the precipitates are effective obstacles to the motion of dislocations, they impede relaxation of internal stresses caused by the strain incompatibility associated with the deformation band. The high internal stresses would then promote the plastic strain transfer to the neighboring sites, i.e., propagation of a deformation band. This conjecture is confirmed by the data of microstructure analysis after tensile tests. Indeed, it can be seen in TEM microphotographs (Figure 9) that both in CG and UFG materials, the Al_3(Sc,Zr) particles are mostly located in the vicinity or directly on the dislocations, while the areas free of dislocations contain few of them.

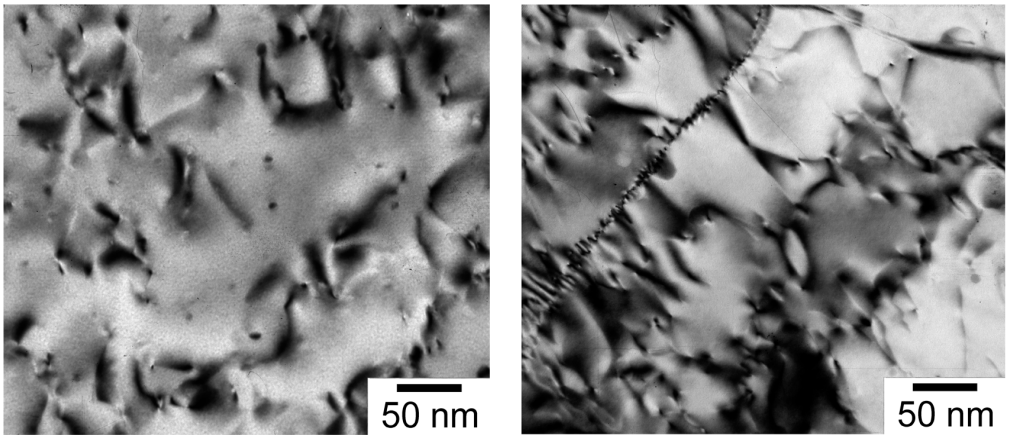

Figure 9. Microstructure of the 5024 alloy deformed till failure at 10^{-3} s^{-1}: (**a**) coarse-grained state; (**b**) after ECAP. The TEM foils were cut approximately 10 mm far from fracture.

The same logic could have been applied to anticipate the possible role of grain boundaries as obstacles to the dislocation motion. However, the results obtained in the present work show that the proneness to the propagation mode, demonstrated by the initial CG material, was weakened by the grain refinement. Indeed, the quasi-continuous mode of band propagation changed to a relay race at high strain rates, and no propagation was observed at low strain rates. It can be suggested that the main role of grain boundaries in the observed peculiarities of the manifestations of the PLC effect is to facilitate the internal stress relaxation, e.g., by serving as sources of dislocations. A general scheme that allows for the transition between the static and propagation modes of kinematics of the PLC bands was proposed earlier (e.g., [45]). Omitting for the sake of simplicity other aspects than that associated with the internal stresses, the following mechanism can be suggested. If the relaxation of the incompatibility stresses is insufficient, be it because of the fast reloading (high strain rate) or a high density of obstacles to the dislocation motion, the local stress state will constantly be heterogeneous but close to the instability threshold all over the sample. Consequently, an excess of the internal stress would result in the propagation of a relatively weak strain localization. In the opposite case, the efficient relaxation of the incompatibility stresses would provide strain uniformization in the specimen. On the one hand, the instability conditions will only be reached when the applied stress approaches the critical level. On the other hand, breakthrough of dislocations in one site would result in a catastrophic process. It could have involved the whole specimen but the elastic reaction of the deformation machine would lead to an abrupt decrease in the stress and stop the further development of the instability. This scenario of collective dynamics of dislocations is analogous to the phenomenon of synchronization in extended dynamical systems [46]. The data presented in Section 3.3 testify that the transition between the synchronization and propagation modes is continuous and gives rise to diverse patterns including the relay-race propagation. This conjecture is confirmed, in particular, by

the observation of progressive changes in the κ-value when the strain rate and/or microstructure are varied. The suggested mechanism also allows for applying the same approach to explain the unusual persistence of type *B* behavior in the fine-grained state, so that the transition to type *A* is not fully accomplished even at a very high strain rate. Such an effect may occur in the conditions when the grain boundaries facilitate stress relaxation in the UFG material.

It should be underlined that not only specific behavior would depend on the subtle balance between different modes of the collective dynamics of dislocations, but the grain boundaries themselves may play a complex role including nucleation, drainage, or pinning of dislocations. The comparison with literature data leads to a suggestion that the resulting behavior depends on the specific microstructure conditions. For example, the preliminary data on the effect of grain refinement on the PLC instability in the alloy studied in [21] bear evidence that the mode of continuous propagation may persist after ECAP [47]. On the other hand, the suppression of the PLC effect after ECAP of a binary alloy was explained in [26] in terms of the worsening of the conditions for synchronization of dislocations.

5. Conclusions

In summary, spatiotemporal behavior of the PLC effect was investigated at room temperature in an AlMgMnScZr alloy with different microstructures and at various strain rates. The coarse-grained material demonstrates atypical behavior characterized by quasi-continuous propagation of deformation bands which persists in the entire strain-rate range. The extensive grain refinement by ECAP breaks such propagation which gives place to a relay race of deformation bands at high or intermediate strain rates and static bands at low strain rates. It also leads to the occurrence of a yield plateau which is superimposed with type *B* stress oscillations and proceeds via sequential nucleation of PLC bands along the tensile axis. The PLC effect is also manifested during necking which occurs in a similar way in both the CG and UFG conditions. Namely, necking is not associated with a persisting localization of plastic deformation but with repeated formation of deformation bands in the necked region.

Although the overall behavior differs in both cases from that observed in binary Al-Mg alloys, all these patterns can be integrated into a general scheme rationalized in terms of a competition between synchronization of dislocations, leading to strain localization when the local strain field is sufficiently uniform, and propagation of plastic activity in heterogeneous strain conditions. One of the factors controlling this balance is the efficiency of relaxation of internal stresses which is affected by both precipitates and grain boundaries. Consequently, the precise manifestations of the PLC instability in alloys with complex compositions may be system-specific and will require a systematic study of various alloys.

Acknowledgments: The authors thank M. Jrad for providing the DIC setup and valuable consultations. The study was financially supported by the Russian Science Foundation, under grant No. 14.584.21.0023 (ID number RFMEFI58417X0023).

Author Contributions: All co-authors contributed to the design of the experimental plan. A.M., D.Y. and R.K. contributed material and realized microstructure experiments. T.L. and M.L. proposed and performed mechanical testing and local extensometry, in cooperation with D.Z. and D.Y., and implemented computer codes for construction of the local strain-rate maps. D.Z. realized the data treatment. D.Z. and M.L. wrote the paper, with contributions and feedback from all co-authors.

Conflicts of Interest: The authors declare no conflict of interest. The founding sponsors had no role in the design of the study; in the collection, analyses, or interpretation of data; in the writing of the manuscript, and in the decision to publish the results.

References

1. Portevin, A.; Le Chatelier, F. Sur un Phénomène Observé lors de L'essai de Traction d'Alliages en Cours de Transformation. *C. R. Acad. Sci. Paris* **1923**, *176*, 507–510.
2. Rodriguez, P. Serrated plastic flow. *Bull. Mater. Sci.* **1984**, *6*, 653–663. [CrossRef]

3. Van den Beukel, A. Theory of the effect of dynamic strain ageing on mechanical properties. *Phys. Status Solidi* **1975**, *30*, 197–206. [CrossRef]
4. Kubin, L.P.; Estrin, Y. The Portevin-Le Chatelier effect in deformation with constant stress rate. *Acta Metall.* **1985**, *33*, 397–407. [CrossRef]
5. Robinson, J.M.; Shaw, M.P. Microstructural and Mechanical Influences on Dynamic Strain Aging Phenomena. *Int. Mater. Rev.* **1994**, *39*, 113–122. [CrossRef]
6. Picu, R.C. A mechanism for the negative strain-rate sensitivity of dilute solid solutions. *Acta Mater.* **2004**, *52*, 3447–3458. [CrossRef]
7. Aboulfadl, H.; Deges, J.; Choi, P.; Raabe, D. Dynamic strain aging studied at the atomic scale. *Acta Mater.* **2015**, *86*, 34–42. [CrossRef]
8. Lebyodkin, M.; Dunin-Barkowskii, L.; Brechet, Y.; Estrin, Y.; Kubin, L.P. Spatio-temporal dynamics of the Portevin-Le Chatelier effect: Experiment and modelling. *Acta Mater.* **2000**, *48*, 2529–2541. [CrossRef]
9. Bharathi, M.S.; Lebyodkin, M.; Ananthakrishna, G.; Fressengeas, C.; Kubin, L.P. The hidden order behind jerky flow. *Acta Mater.* **2002**, *50*, 2813–2824. [CrossRef]
10. Robinson, J.M. Serrated flow in aluminium base alloys. *Int. Mater. Rev.* **1994**, *39*, 217–227. [CrossRef]
11. Balik, J.; Lukac, P. Portevin-Le Chatelier instabilities in Al-3Mg alloy conditioned by strain rate and strain. *Acta Metall. Mater.* **1993**, *41*, 1447–1454. [CrossRef]
12. Chihab, K.; Estrin, Y.; Kubin, L.P.; Vergnol, J. The kinetics of the Portevin-Le Chatelier bands in an Al-5at%Mg alloy. *Scr. Mater.* **1987**, *21*, 203–208. [CrossRef]
13. Horvath, G.; Chinh, N.Q.; Gubicza, J.; Lendvai, J. Plastic instabilities and dislocation densities during plastic deformation in Al-Mg alloys. *Mater. Sci. Eng. A* **2007**, *445–446*, 186–192. [CrossRef]
14. Halim, H.; Wilkinson, D.S.; Niewczas, M. The Portevin-Le Chatelier (PLC) effect and shear band formation in an AA5754 alloy. *Acta Mater.* **2007**, *55*, 4151–4160. [CrossRef]
15. Louche, H.; Vacher, P.; Arrieux, R. Thermal observations associated with the Portevin-Le Chatelier effect in an Al-Mg alloy. *Mater. Sci. Eng. A* **2005**, *404*, 188–196. [CrossRef]
16. Jiang, H.; Zhang, Q.; Chen, X.; Chen, Z.; Jiang, Z.; Wu, X.; Fan, J. Three types of Portevin-Le Chatelier effect: Experiment and modeling. *Acta Mater.* **2007**, *55*, 2219–2228. [CrossRef]
17. Lebyodkin, M.A.; Lebedkina, T.A. Multifractality and randomness in the unstable plastic flow near the lower strain-rate boundary of instability. *Phys. Rev. E* **2008**, *77*, 026111. [CrossRef] [PubMed]
18. Kok, S.; Beaudoin, A.J.; Tortorelli, D.A.; Lebyodkin, M. A finite element model for the Portevin-Le Chatelier effect based on polycrystal plasticity. *Model. Simul. Mater. Sci. Eng.* **2002**, *10*, 745–763. [CrossRef]
19. Polmear, I.J. *Light Alloys: From Traditional Alloys to Nanocrystals*, 4th ed.; Butterworth-Heinemann/Elsevier: Oxford, UK, 2006; pp. 205–235. ISBN 978-0-75-066371-7.
20. Filatov, Y.A.; Yelagin, V.I.; Zakharov, V.V. New Al-Mg-Sc alloys. *Mater. Sci. Eng. A* **2000**, *280*, 97–101. [CrossRef]
21. Zhemchuzhnikova, D.A.; Lebyodkin, M.A.; Lebedkina, T.A.; Kaibyshev, R.O. Unusual behavior of the Portevin-Le Chatelier effect in an AlMg alloy containing precipitates. *Mater. Sci. Eng. A* **2015**, *639*, 37–41. [CrossRef]
22. Estrin, Y.; Vinogradov, A. Extreme grain refinement by severe plastic deformation: A wealth of challenging science. *Acta Mater.* **2013**, *61*, 782–817. [CrossRef]
23. Sabirov, I.; Murashkin, M.Y.; Valiev, R.Z. Nanostructured aluminium alloys produced by severe plastic deformation: New horizons in development. *Mater. Sci. Eng. A* **2013**, *560*, 1–24. [CrossRef]
24. Malopheyev, S.; Kaibyshev, R. Strengthening mechanisms in a Zr-modified 5083 alloy deformed to high strains. *Mater. Sci. Eng. A* **2015**, *620*, 246–252. [CrossRef]
25. Mogucheva, A.; Yuzbekova, D.; Kaibyshev, R.; Lebedkina, T.; Lebyodkin, M. Effect of grain refinement on jerky flow in Al-Mg-Sc alloy. *Metall. Mater. Trans. A* **2016**, *47*, 2093–2106. [CrossRef]
26. Lebedkina, T.A.; Lebyodkin, M.A.; Lamark, T.T.; Janecek, M.; Estrin, Y. Effect of equal channel angular pressing on the Portevin-Le Chatelier effect in an Al3Mg alloy. *Mater. Sci. Eng. A* **2014**, *615*, 7–13. [CrossRef]
27. Zhao, S.; Meng, C.; Mao, F.; Hu, W.; Gottstein, G. Influence of severe plastic deformation on dynamic strain aging of ultrafine grained Al-Mg alloys. *Acta Mater.* **2014**, *76*, 54–67. [CrossRef]
28. Mogucheva, A.; Babich, E.; Ovsyannikov, B.; Kaibyshev, R. Microstructural evolution in a 5024 aluminum alloy processed by ECAP with and without back pressure. *Mater. Sci. Eng. A* **2013**, *560*, 178–192. [CrossRef]

29. Valiev, R.Z.; Langdon, T.G. Principles of equal-channel angular pressing as a processing tool for grain refinement. *Prog. Mater. Sci.* **2006**, *51*, 881–981. [CrossRef]
30. Lebedkina, T.A.; Lebyodkin, M.A.; Château, J.-P.; Jacques, A.; Allain, S. On the mechanism of unstable plastic flow in an austenitic FeMnC TWIP steel. *Mater. Sci. Eng. A* **2009**, *519*, 147–154. [CrossRef]
31. Cai, Y.L.; Yang, S.L.; Wang, Y.H.; Fu, S.H.; Zhang, Q.C. Characterization of the deformation behaviors associated with the serrated flow of a 5456 Al-based alloy using two orthogonal digital image correlation systems. *Mater. Sci. Eng. A* **2016**, *664*, 155–164. [CrossRef]
32. Lebedkina, T.A.; Lebyodkin, M.A. Effect of deformation geometry on the intermittent plastic flow associated with the Portevin-Le Chatelier effect. *Acta Mater.* **2008**, *56*, 5567–5574. [CrossRef]
33. Kral, R.; Lukac, P. Modelling of strain hardening and its relation to the onset of Portevin-Le Chatelier effect in Al-Mg alloys. *Mater. Sci. Eng. A* **1997**, *234–236*, 786–789. [CrossRef]
34. Schwab, R.; Ruff, V. On the nature of the yield point phenomenon. *Acta Mater.* **2013**, *61*, 1798–1808. [CrossRef]
35. Antolovich, S.D.; Armstrong, R.W. Plastic strain localization in metals: Origins and consequences. *Prog. Mater. Sci.* **2014**, *59*, 1–160. [CrossRef]
36. Kubin, L.P.; Estrin, Y. Evolution of dislocation densities and the critical conditions for the Portevin-Le Chatelier effect. *Acta Metall. Mater.* **1990**, *38*, 697–708. [CrossRef]
37. Nijs, O.; Holmedal, B.; Friis, J.; Nes, E. Sub-structure strengthening and work hardening of an ultra-fine grained aluminium-magnesium alloy. *Mater. Sci. Eng. A* **2008**, *483–484*, 51–53. [CrossRef]
38. Coër, J.; Manach, P.Y.; Laurent, H.; Oliveira, M.C.; Menezes, L.F. Piobert-Lüders plateau and Portevin-Le Chatelier effect in an Al-Mg alloy in simple shear. *Mech. Res. Commun.* **2013**, *48*, 1–7. [CrossRef]
39. Klusemann, B.; Fischer, G.; Böhlke, T.; Svendsen, G.B. Thermomechanical characterization of Portevin-Le Chatelier bands in AlMg3 (AA5754) and modeling based on a modified Estrin-McCormick approach. *Int. J. Plast.* **2015**, *67*, 192–216. [CrossRef]
40. Ait-Amokhtar, H.; Vacher, P.; Boudrahem, S. Kinematics fields and spatial activity of Portevin-Le Chatelier bands using the digital image correlation method. *Acta Mater.* **2006**, *54*, 4365–4371. [CrossRef]
41. Yuzbekova, D.; Mogucheva, A.; Zhemchuzhnikova, D.; Lebedkina, T.; Lebyodkin, M.; Kaibyshev, R. Effect of microstructure on continuous propagation of the Portevin-Le Chatelier deformation bands. *Int. J. Plast.* **2017**, *96*, 210–226. [CrossRef]
42. Zuev, L.B. On the waves of plastic flow localization in pure metals and alloys. *Ann. Phys.* **2007**, *16*, 286–310. [CrossRef]
43. Mudrock, R.N.; Lebyodkin, M.A.; Kurath, P.; Beaudoin, A.J.; Lebedkina, T.A. Strain-rate fluctuations during macroscopically uniform deformation of a solution-strengthened alloy. *Scr. Mater.* **2011**, *65*, 1093–1096. [CrossRef]
44. Fressengeas, C.; Beaudoin, A.J.; Entemeyer, D.; Lebedkina, T.; Lebyodkin, M.; Taupin, V. Dislocation transport and intermittency in the plasticity of crystalline solids. *Phys. Rev. B* **2009**, *7*, 014108. [CrossRef]
45. Lebyodkin, M.A.; Kobelev, N.P.; Bougherira, Y.; Entemeyer, D.; Fressengeas, C.; Gornakov, V.S.; Lebedkina, T.A.; Shashkov, I.V. On the similarity of plastic flow processes during smooth and jerky flow: Statistical analysis. *Acta Mater.* **2012**, *60*, 3729–3740. [CrossRef]
46. Pérez, C.J.; Corral, Á.; Díaz-Guilera, A.; Christensen, K.; Arenas, A. On self-organized criticality and synchronization in lattice models of coupled dynamical systems. *Int. J. Mod. Phys. B* **1996**, *10*, 1111–1151. [CrossRef]
47. Zhemchuzhnikova, D.A.; Lebyodkin, M.A.; Lebedkina, T.A.; Kaibyshev, R.O. The Portevin-Le Chatelier Effect and Kinematics of Deformation Bands in an Al-Mg-Sc Alloy: Effect of Grain Size. *Mater. Sci. Forum* **2016**, *879*, 2268–2273. [CrossRef]